Electronic Supplementary Material (ESI) for Journal of Materials Chemistry C.

Electronic Supplementary Information

Position of Gold Dictates the Photophysical and Photocatalytic Properties of Cu_2O in Cu_2O/Au Multicomponent Nanoparticles

*Dávid Kovács, András Deák, György Z. Radnóczi, Zsolt E. Horváth, Attila Sulyok, Róbert Schiller, Ottó Czömpöly, Dániel Zámbó**

Centre for Energy Research, Budapest, Hungary

E-mail: daniel.zambo@ek-cer.hu

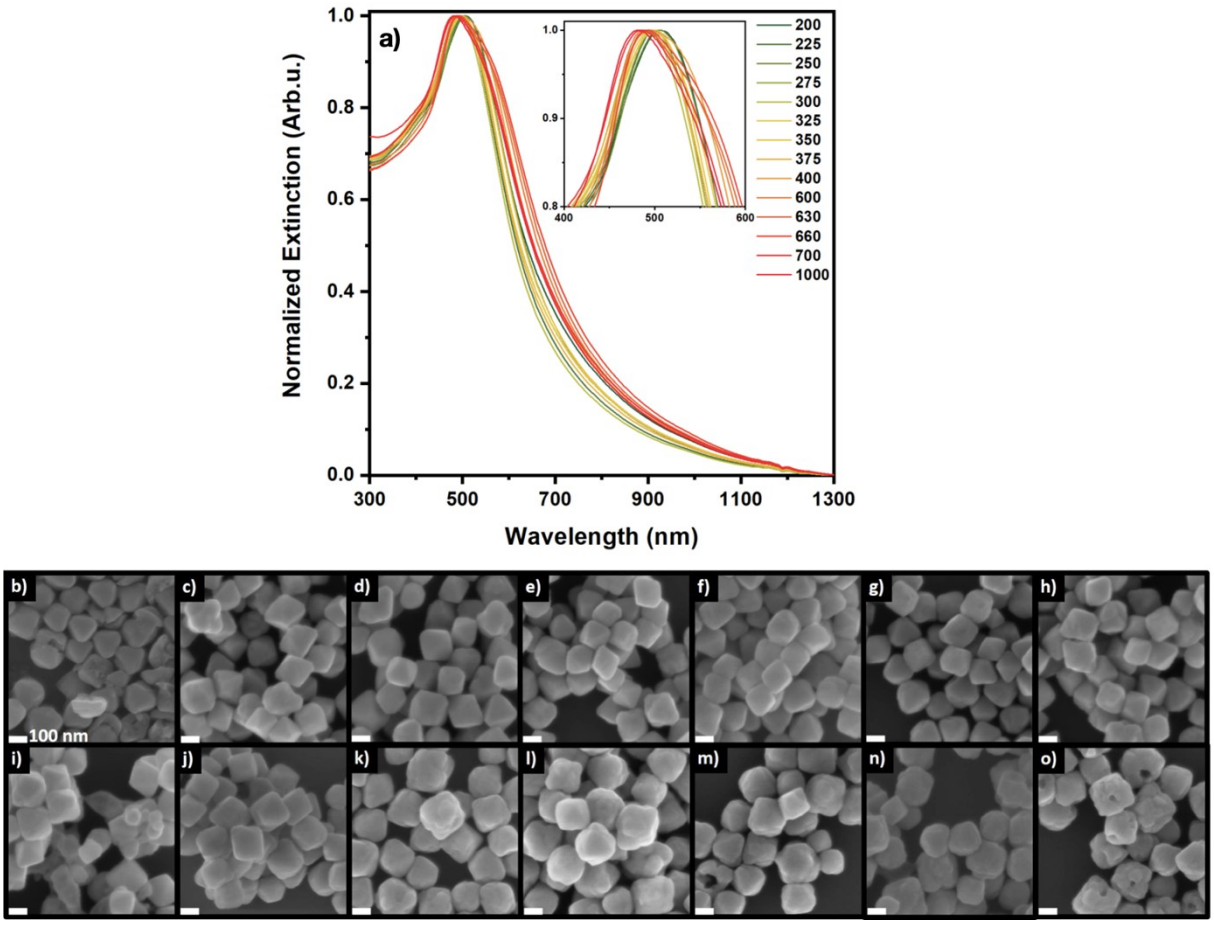

Figure S1. Spectral (a) and morphological (b-o) changes of the Cu_2O nanooctahedra upon adjusting the hydrazine concentration (i.e. added volumes in μL) in the synthesis. SEM images (b-o) correspond to the increasing volumes of N_2H_4 from 200 μL (b) to 1000 μL (o). Scale bars represent 100 nm.

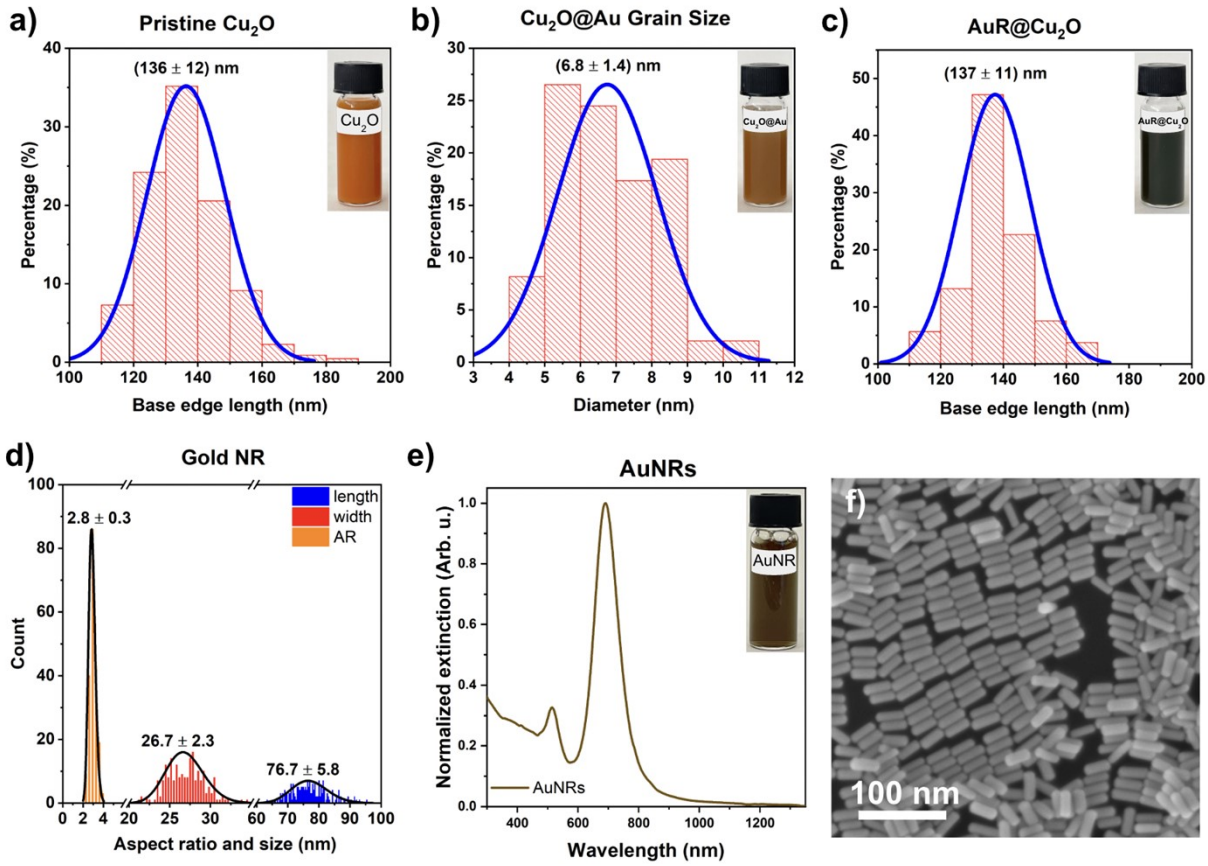

Figure S2. Size distribution of the synthesized nanoparticles. Base edge length distribution of pristine Cu_2O nanooctahedra (a), size distribution of AuNGs in Cu_2O@Au octahedra (b), aspect ratio, width and length distribution of the synthesized AuNRs (c), and base edge length distribution of AuR@Cu_2O octahedra (d).

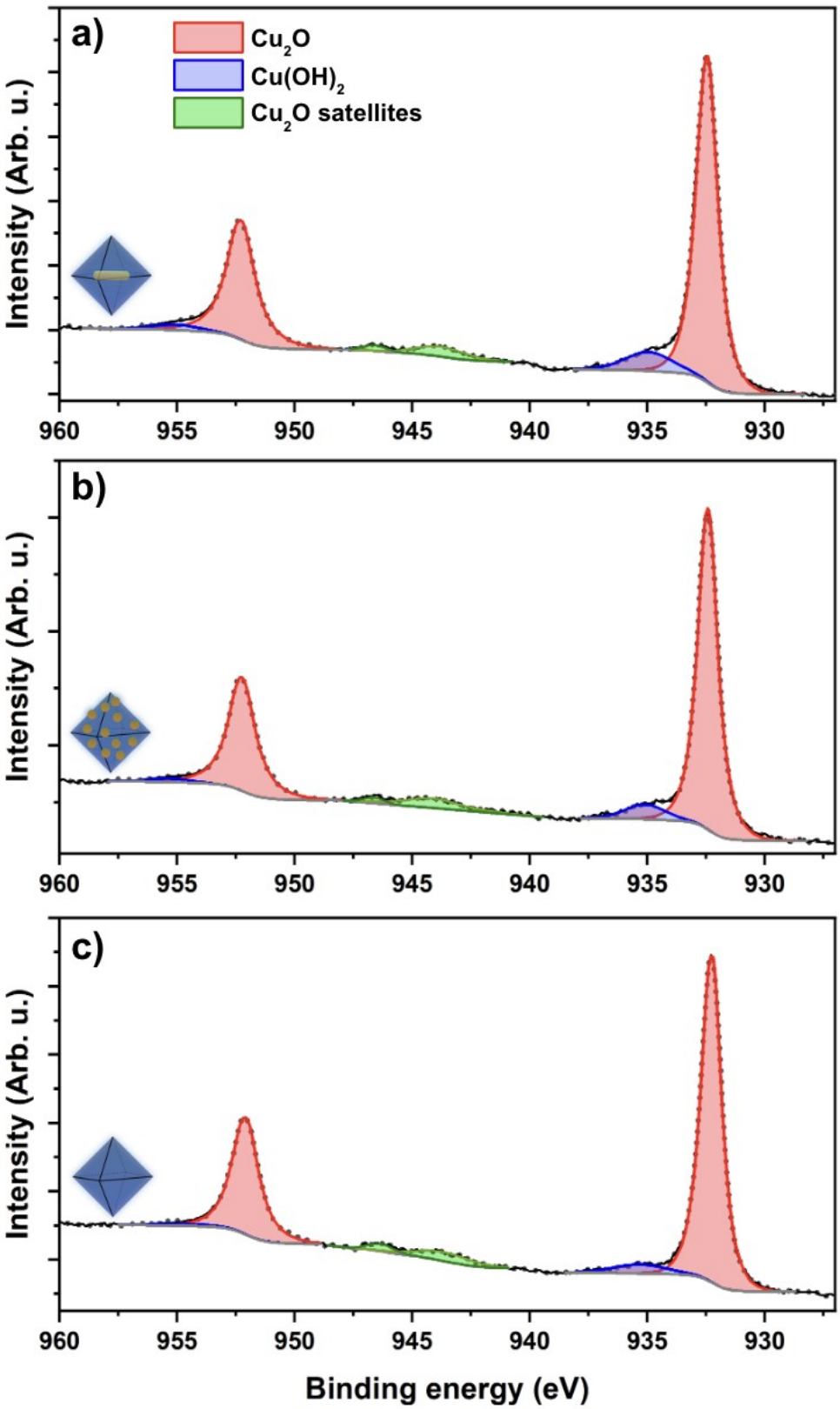

Figure S3. Decomposition of Cu $2p_{1/2}$, satellites and $2p_{3/2}$ peaks of AuR@Cu_2O (a), Cu_2O@Au (b) and pristine Cu_2O (c) measured by XPS. It shows a weak contribution of $Cu(OH)_2$ (blue fitted curves). Since the Cu_2O is synthesized in aqueous medium a residue of

hydroxyl at the uppermost layer can be reasonably assumed which makes its contribution overrepresented in the XPS signal. On the intensity axes, major ticks represent 20000 counts.

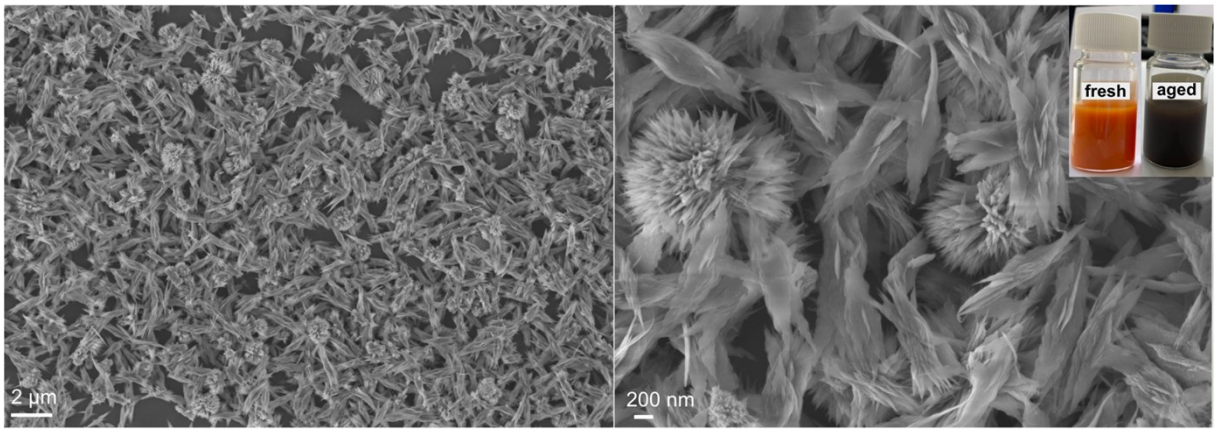

Figure S4. Aging dramatically changes the morphology of the Cu_2O nanooctahedra. The SEM images show the morphological change after 1 week. Inset shows the color change of the solution from orange (freshly prepared sample) to black (after 1 week, stored in water).

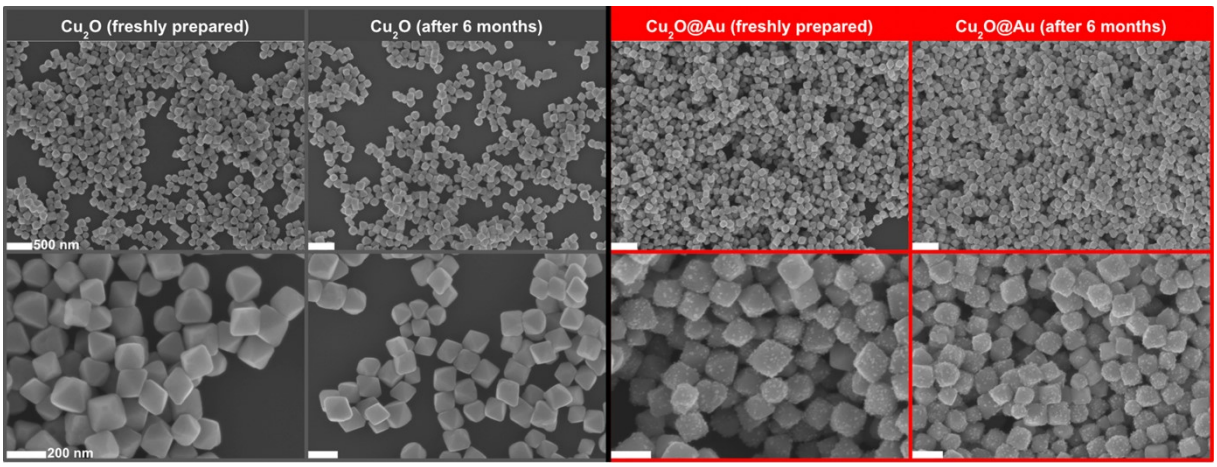

Figure S5. Effect of storage in ethanolic medium on the particle morphology for Cu_2O octahedra (left, grey) and Cu_2O@Au heteroparticles (right, red). The particles remain intact even up to 6 months of shelf life.

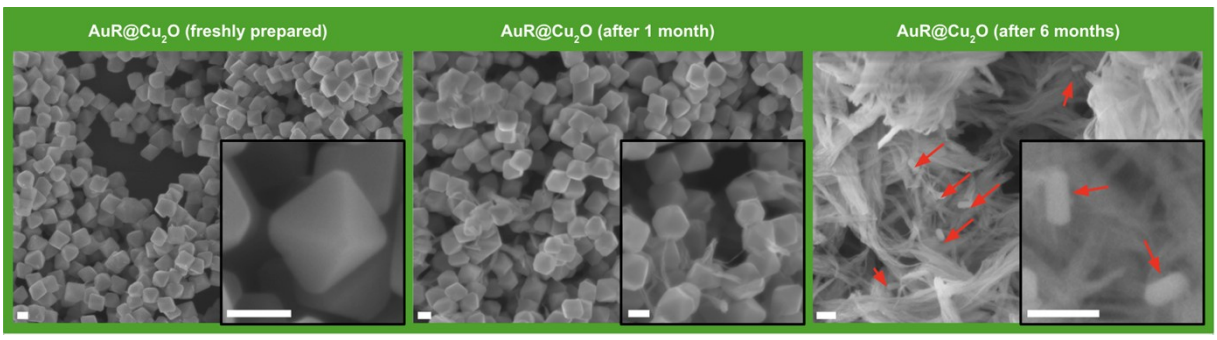

Figure S6. Effect of storage in ethanolic medium and at ambient conditions on the particle morphology for AuR@Cu_2O particles in time. Upon storing the samples at room temperature and exposed to ambient light, the particles start to be oxidized and fully degrade in several months. Red arrows show the gold nanorods within the CuO matrix. Scale bars represent 100 nm.

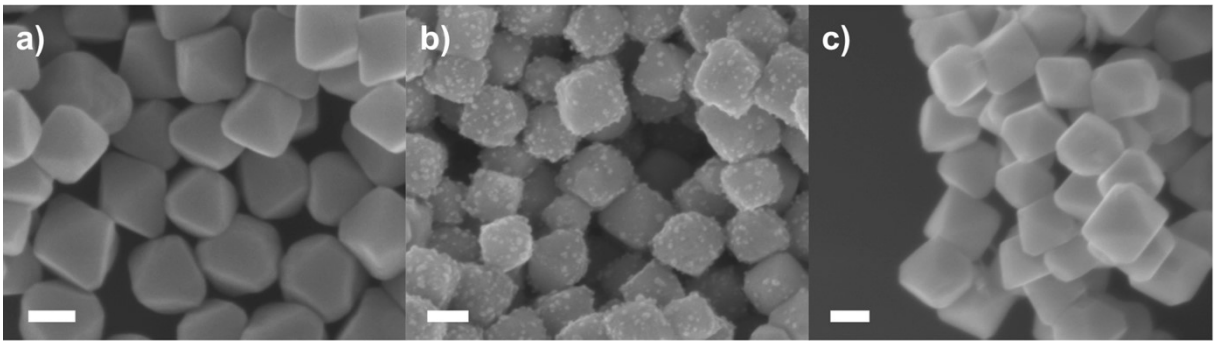

Figure S7. Effect of storage of the dried nanoparticle films on the morphology: Cu_2O (a, 6 months), Cu_2O@Au (b, 6 months), and AuR@Cu_2O (c, 2 months).

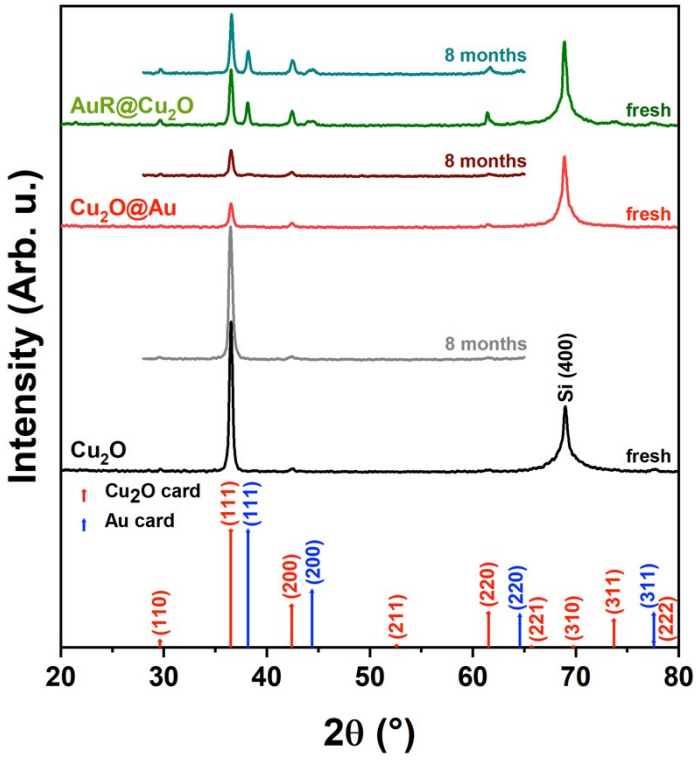

Figure S8. Effect of storage at ambient conditions on the XRD diffractograms of the nanoparticle films. The peak at 69.2° corresponds to the Si{400} diffraction of the applied silicon substrate.

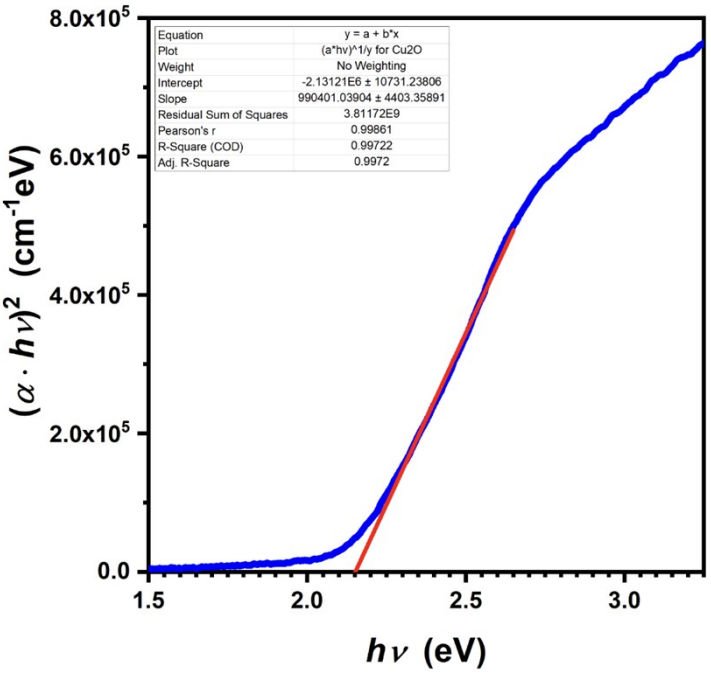

Figure S9. Tauc plot of the ethanolic Cu_2O nanooctahedra solution. The absorbance of the ethanolic solution of the pristine Cu_2O nanoparticles was converted to $(\alpha \cdot h\nu)^2$, where h is the Planck constant, ν is the frequency, and α is the molar absorption coefficient of the particle solution calculated based on the concentration of copper-oxide in the solution ($c(Cu_2O)$ = 0.5 mM). The exponent is 2 for semiconductors with a direct band gap. The intersection of the linear fit and the x-axis gives the band gap (2.15 eV).

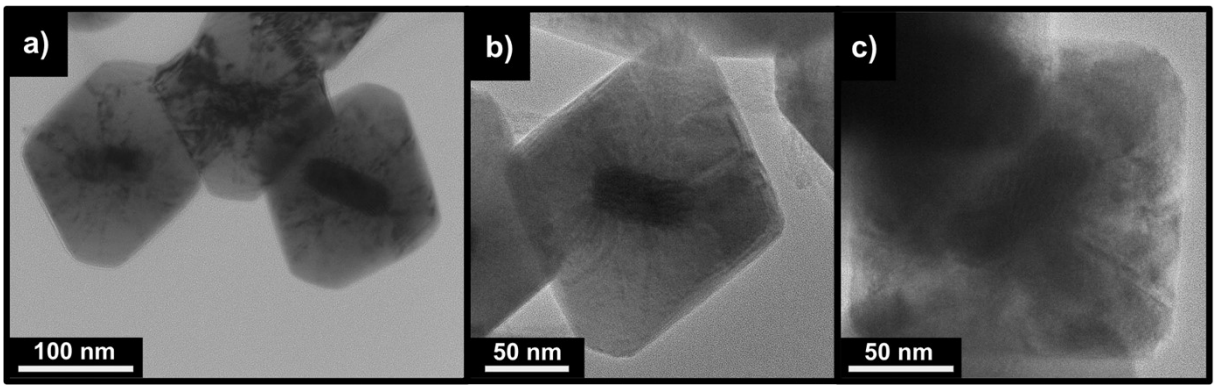

Figure S10. TEM images showing the stress-induced crystal defects in AuR@Cu_2O nanoooctahedra.

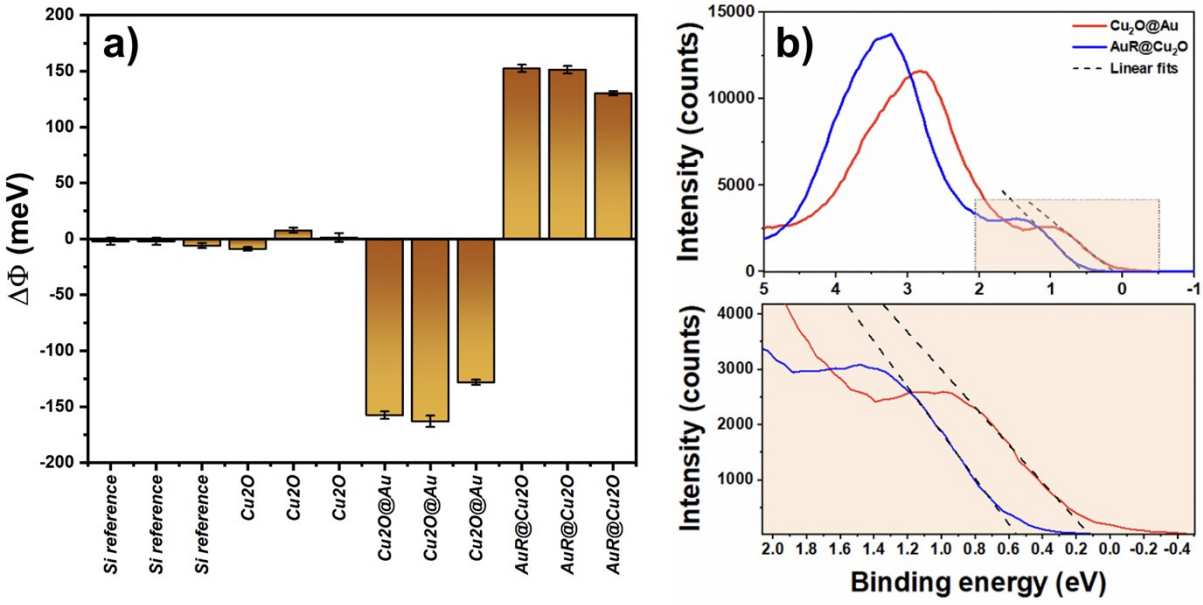

Figure S11. Contact potential differences measured by single-point Kelvin probe (a) and valence band spectra (measured by XPS) of the nanoparticle films (b). Enlarged area in panel b shows the linear fitting to determine the valence band maxima.

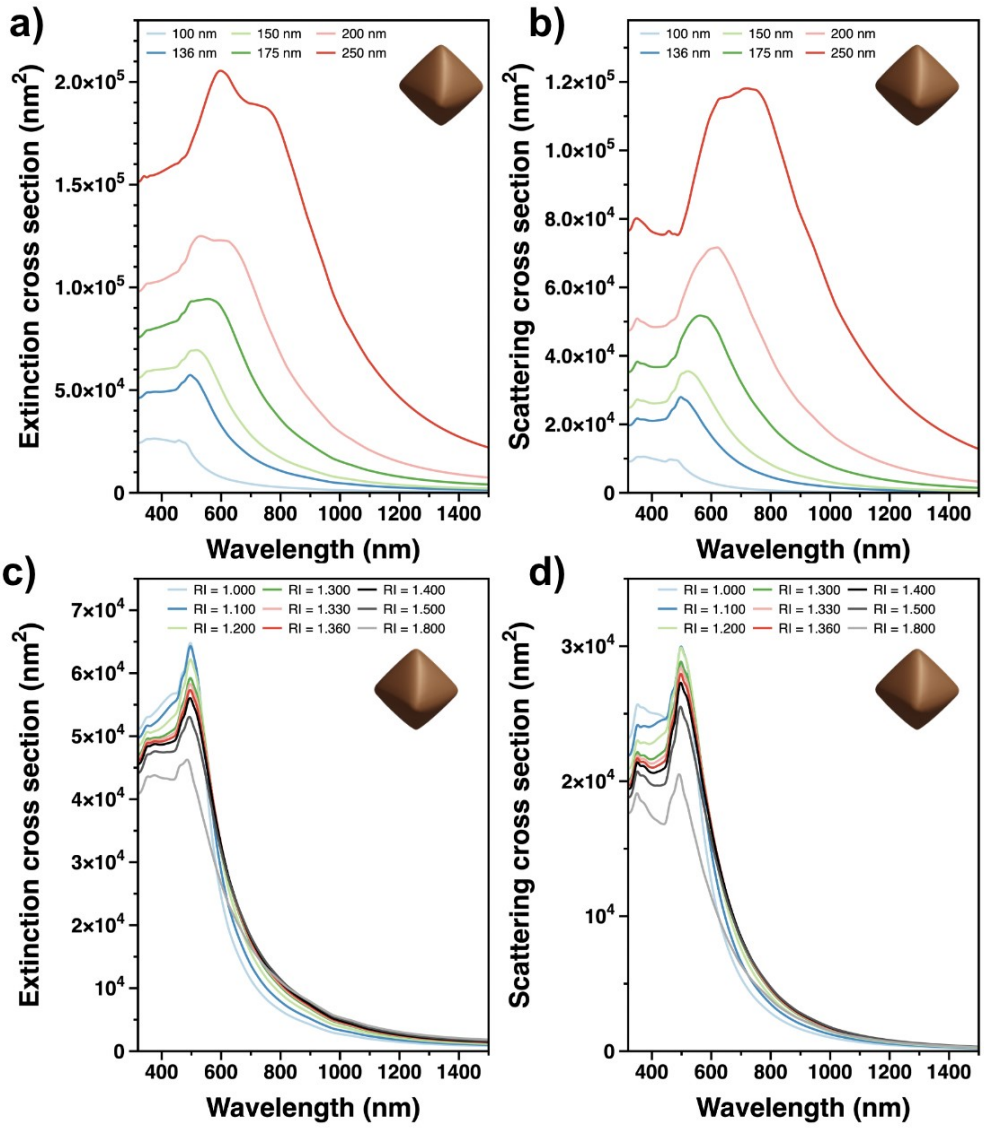

Figure S12. Calculated extinction (a,c) and scattering cross sections (b,d) for a pristine Cu_2O octahedron upon changing the size of the particle (a,b) and the refractive index (RI) of the embedding medium (c,d).

The extinction and scattering of an ethanol-filled cavity in bulk Cu_2O do not feature any peak in the spectra (Figure S13). Nevertheless, surface charge distribution plots at 670 nm indicate a dipolar cavity mode with small cross section. Interestingly, if the cavity is filled with gold (*i.e.* an AuNR is embedded in an infinite Cu_2O matrix), a new resonant mode appears: a superposition of a hexapolar cavity mode and the dipolar resonance of the NR (Figure S14c-d). A weak hexapolar cavity mode can also be observed in the octahedral-shaped particle with an EtOH-filled cavity (Figure S14g), but it is intensified by the presence of gold due to its higher polarizability. Therefore, in case of an AuR@Cu_2O octahedral particle geometry, the hexapolar cavity mode of the Cu_2O octahedron (Figure 14f) and the transversal dipole mode of the NR

can couple to generate a binding dark mode (Figure S14h). The overlap of this dark mode with the hexapolar cavity and rod transversal modes leads to Fano resonance and hence a resulting spectral dip.

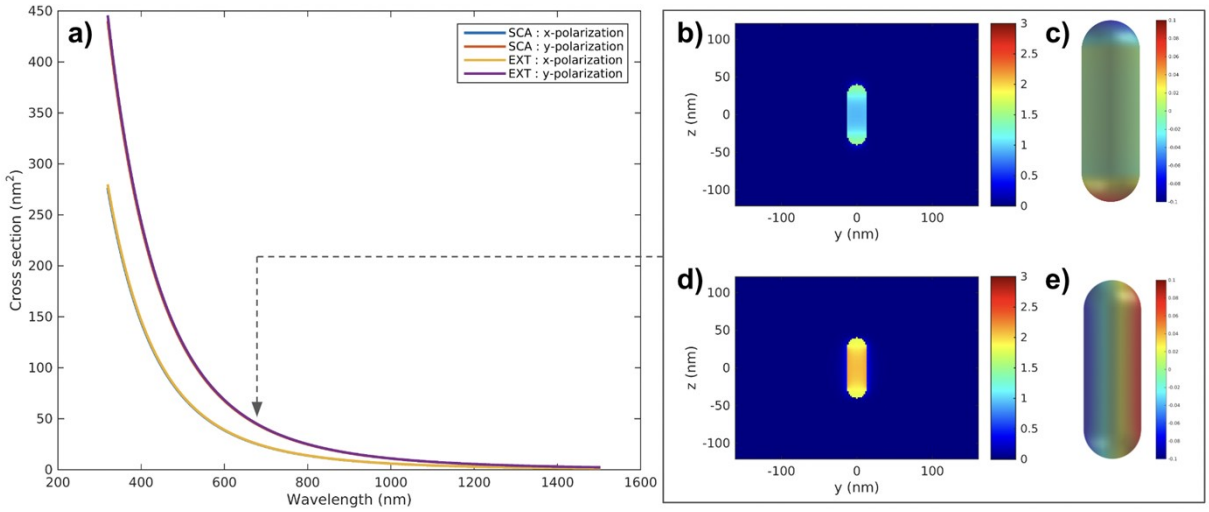

Figure S13. Calculated extinction and scattering cross sections of bulk Cu_2O having an ethanol-filled rod-shaped cavity (a) and the near field plots (b,d) and surface charge distributions (c,e) at 670 nm. Panel b and c correspond to the longitudinal excitation, while d and e correspond to the transversal excitation.

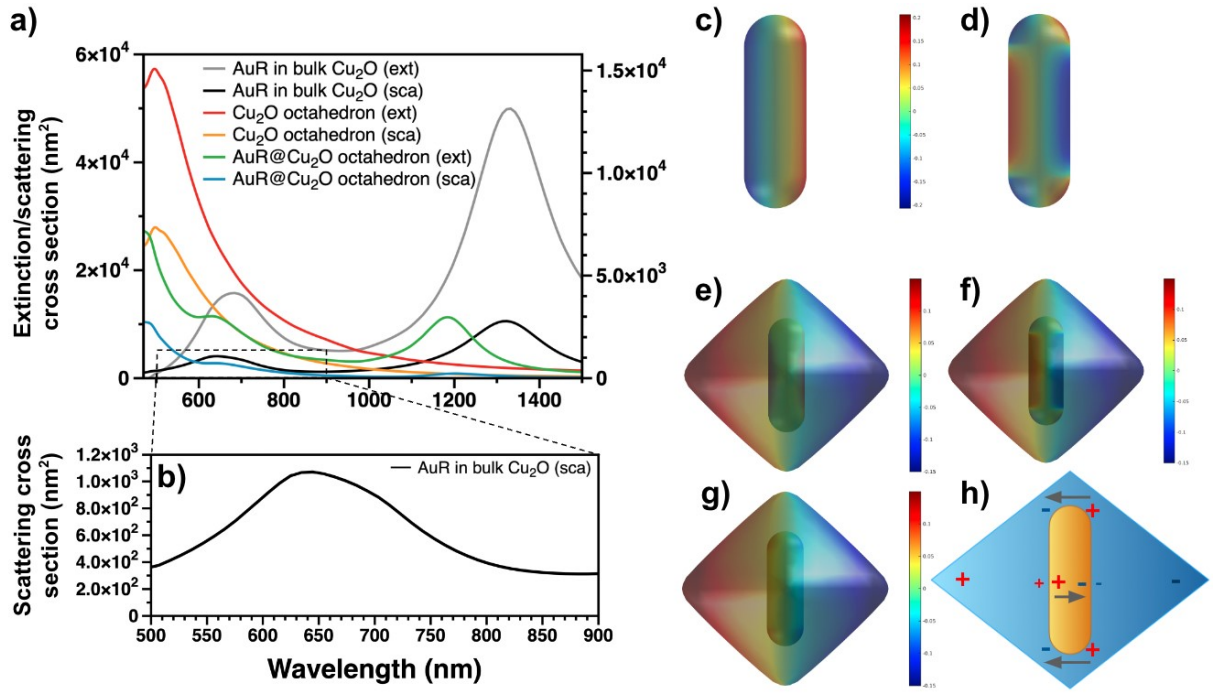

Figure S14. Simulation of extinction (ext) and scattering (sca) cross sections of a single nanooctahedron, an AuNR in bulk Cu_2O and an AuR@Cu_2O octahedron (a). Enlarged region of the simulated scattering spectrum of a AuNR in bulk Cu_2O. Surface charge distribution of AuNR in bulk Cu_2O (c,d) at 550 nm and 670 nm. Surface charge distribution of an

AuR@Cu_2O (e-f) at 580 nm (c,e) and 640 nm (d,f). Surface charge distribution of a Cu_2O octahedron with an ethanol-filled cavity at 640 nm (g). Schematics of the emerging binding dark mode in AuR@Cu_2O at 640 nm (h).

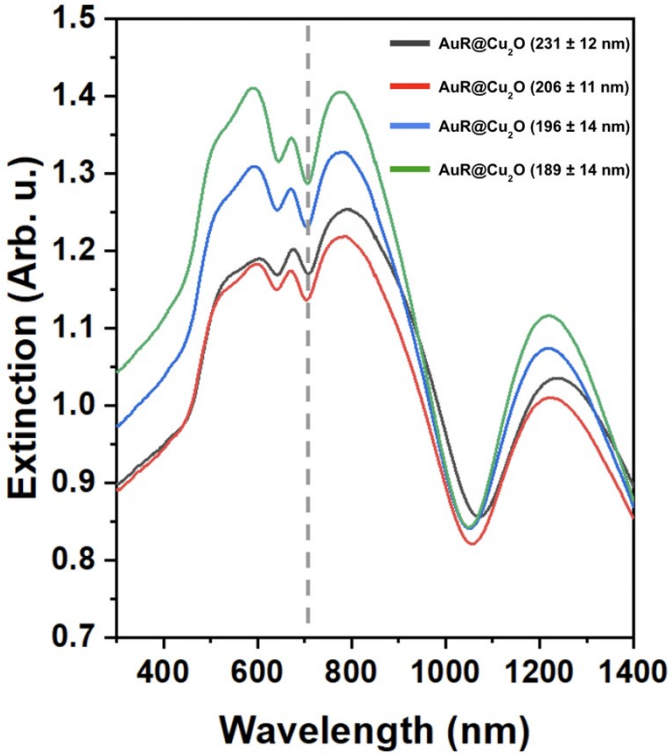

Figure S15. Extinction spectra of differently sized AuR@Cu_2O heterooctahedra synthesized using nanorods with dimensions of 108x43 nm. Changing the edge length of the octahedra does not influence the position of the Fano dip in the spectra (marked with a dashed gray line).

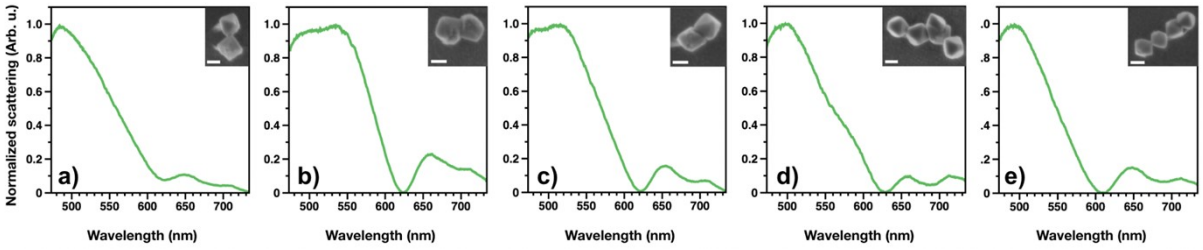

Figure S16. Scattering spectra of the different assemblies (SEM images shown as insets) of AuR@Cu_2O on ITO substrate. Scale bars represent 100 nm.

While heteronanoparticles (Cu_2O@Au and AuR@Cu_2O) showed prominent photocatalytic activity even at the applied low-power illumination source (*i.e.* UV flashlight, 38 mW/cm^2), pristine Cu_2O octahedra were found to be inactive (Figure 7 in the main text). Same behaviour was observed if the particles were illuminated with monochromatic, but low-power He-Cd

laser (λ = 325 nm, expanded beam with a power density of ~40 mW/cm^2). This implies, that the applied sources are not sufficient to make the octahedra active.

Therefore, photocatalytic dye degradation experiment was performed *via* using a higher power LED source (Thorlabs M365LP1 focused to a 1x1 cm square, 800 mA driving current, power density of ~500 mW/cm^2). Although the dye degradation starts to proceed after 120 minutes and reaches a maximum value of 72 %, this accompanies with the complete loss of the octahedral particle morphology. Figure S17 shows the gradual photocorrosion of the Cu_2O particles in time. Illumination leads to octahedra with rough facets (in the first 10 minutes) followed by the evolution of hollow (60-120 minutes) and shapeless particles (180-360 minutes). Thus, it can be concluded that the observed photocatalytic activity is not related to the octahedral shape of the particles.

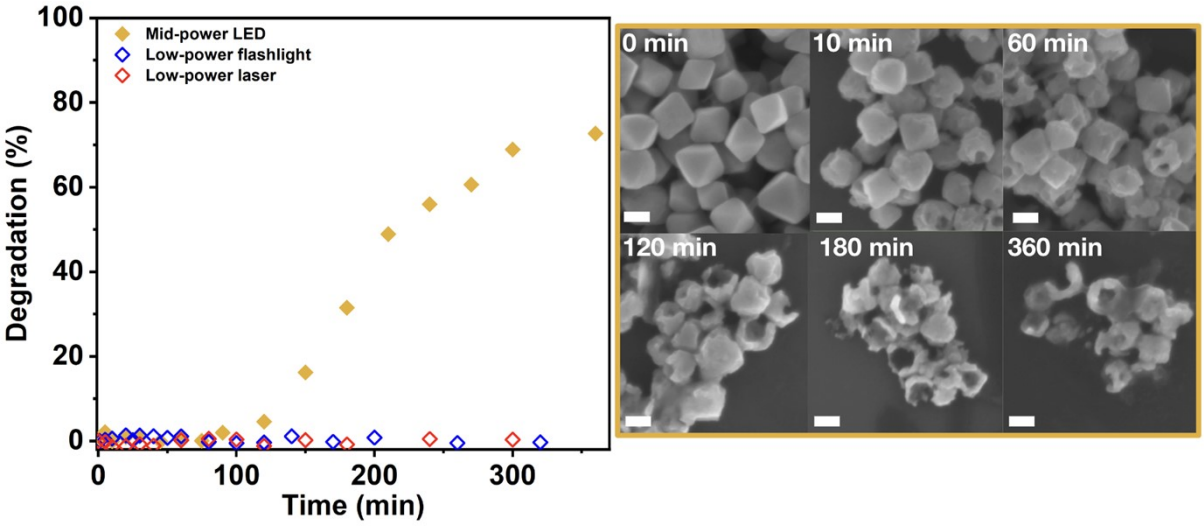

Figure S17. Comparison of degradation kinetics of methyl orange dye in the presence of pristine Cu_2O nanooctahedra upon illuminating the system with low-power sources (flashlight and He-Cd UV laser) or mid-power LED. Although dye degradation is prominent for higher power illumination, SEM images show that intensive photocorrosion of the octahedra can be observed. Scale bars represent 100 nm.

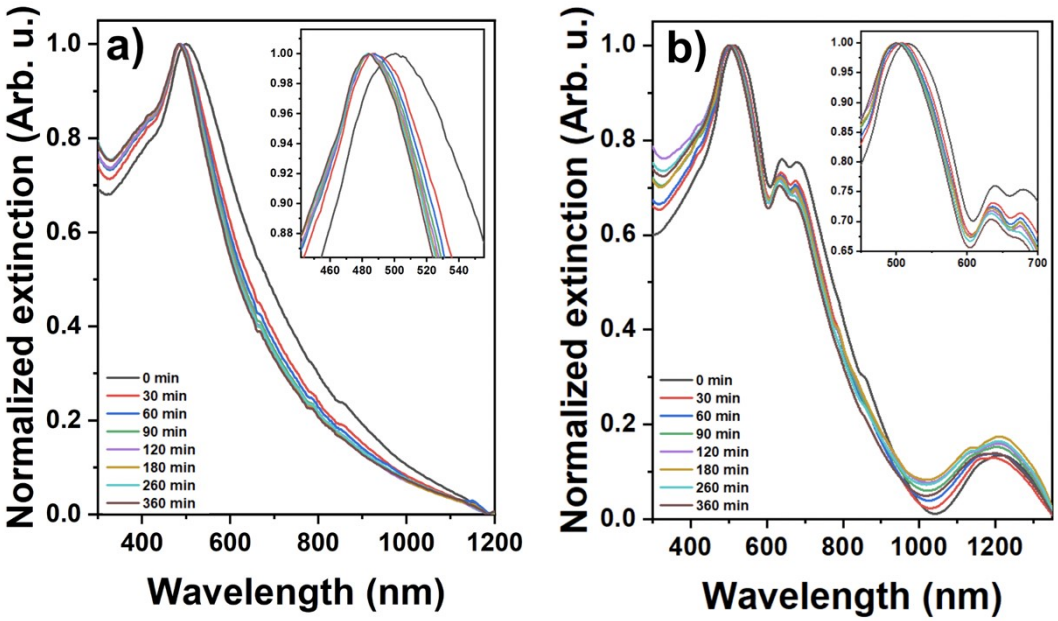

Figure S18. Time-dependent normalized extinction spectra of Cu_2O@Au (a) and AuR@Cu_2O (b) under UV illumination supporting the data in Figure 7 (main text). Insets show enlarged spectral windows to visualize the peak shifts in a more pronounced manner.

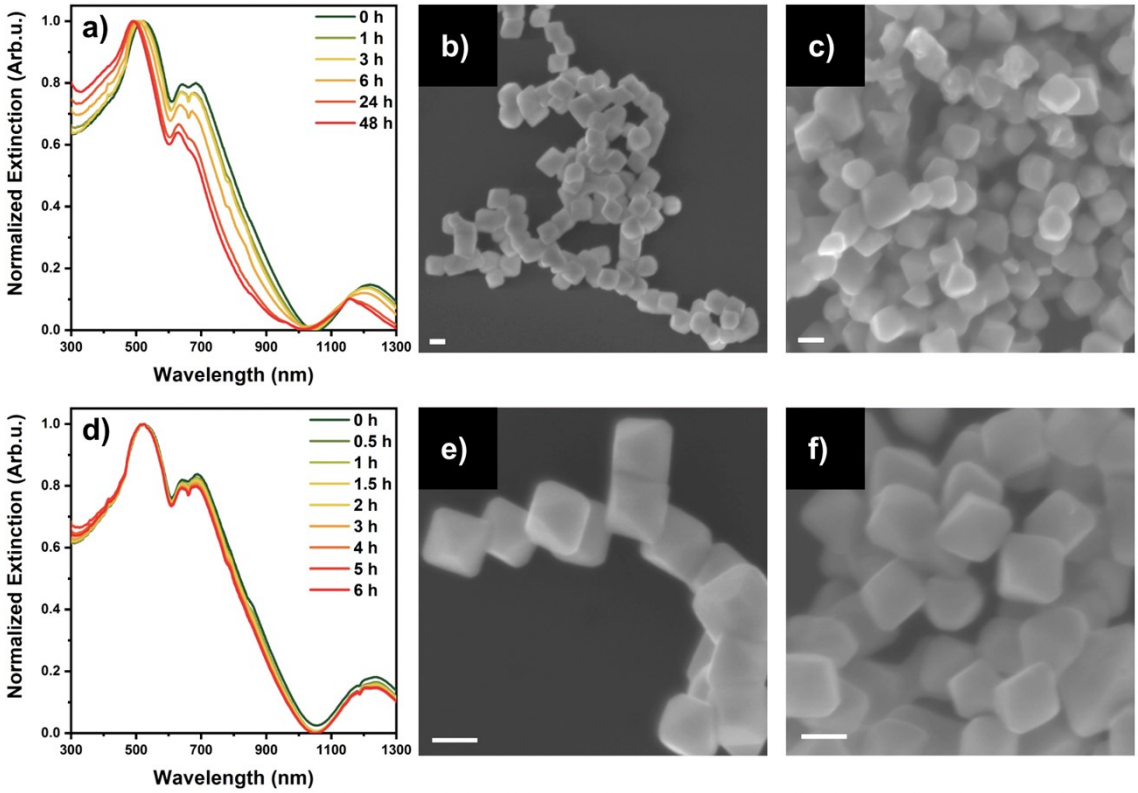

Figure S19. Evolution of the extinction spectra (a,d) and the particle morphology (b,c,e,f) of AuR@Cu_2O particles in different environments: aqueous medium and dark (a) before (b) and after 48 hours (c), ethanolic medium and UV illumination (d, flashlight) before (e) and after 6 hours (f). Scale bars represent 100 nm.